INTERNATIONAL JOURNAL OF INTEGRATED ENGINEERING
ISSN: 2229-838X e-ISSN: 2600-7916

IJIE

Vol. 17 No. 5 (2025) 363-375
https://publisher.uthm.edu.my/ojs/index.php/ijie

Improvement of Preprocessing for Spiral and Wave Handwriting Image Classification Using DenseNet-169

Arizal Mujibtamala Nanda Imron[1]*, Zilvanhisna Emka Fitri[2], Azizatul Mashwafah[2], Wahyu Muldayani[1], Sumardi[3]

[1] *Electrical Engineering Technology, Department of Electrical Enginering, Faculty of Engineering, Universitas Jember, Jember, 68121, INDONESIA*
[2] *Informatics Engineering, Department of Information Technology, Politeknik Negeri Jember, Jember, 68121, INDONESIA*
[3] *Electrical Engineering, Department of Electrical Enginering, Faculty of Engineering, Universitas Jember, Jember, 68121, INDONESIA*

*Corresponding Author: arizal.tamala@unej.ac.id
DOI: https://doi.org/10.30880/ijie.2025.17.05.028

Article Info

Received: 8 January 2025
Accepted: 10 March 2025
Available online: 30 August 2025

Keywords

Computer vision, handwriting, parkinson disease, preprocessing, CNN, DenseNet-169

Abstract

Parkinson's disease (PD) is the second most common neurodegenerative disorder, impacting over 10 million people. Key symptoms include slowed limb movements, difficulty writing, and involuntary tremors. Tremor is the first motor symptom of Parkinson's disease, seen in about 75% of patients. Neurologists assess tremors through various non-invasive tests. This may involve assessing handwriting and spiral drawing. The analysis is still performed manually by neurologists, which can introduce subjectivity. Applications using computer vision techniques should be developed to classify handwriting as healthy or tremor-affected, aiding neurologists in making more objective decisions. DenseNet-169 can classify spiral and wave images in tremor and non-tremor classes with the addition of preprocessing obtained a training accuracy of 100% while the system test accuracy is 93% while without preprocessing, the system accuracy is 81%.

1. Introduction

Parkinson's disease (PD) is a neurodegenerative disorder that affects the central nervous system[1]. It is characterized by resting tremor, rigidity, bradykinesia, and postural instability, which collectively result in disability in patients [2]. Parkinson's disease (PD) is the second most common neurodegenerative illness globally, affecting over 10 million people. Additionally, PD is a disease that progresses gradually, which can make it challenging to diagnose in its initial stages. [3]. The most reported symptoms among PD patients include slowed movement of the extremities, difficulty writing, and involuntary tremors. Tremor represents the earliest motor symptom of PD, with approximately 75% of patients with PD experiencing it. [4]. To ascertain whether the patient is presented with tremors, the neurologist will initially conduct a series of tests utilizing conventional, non-invasive methodologies. These may include assessments of handwriting and the ability to draw spirals on paper [1], [5], [6]. The analysis process is still conducted manually by neurologists, which can lead to subjectivity. To assist the neurologist in this process, it is necessary to develop an application that can utilize computer vision techniques to categorize handwriting as either healthy or affected by tremors, thereby making the decision-making process more objective. Computer vision techniques are now widely applied in a variety of fields, including the health sector.

Computer vision involves the development of computer algorithms that simulate human visual perception and extract information from objects. It is a branch of artificial intelligence that is concerned with the processing

of visual information. There are similarities between the human eye and computer vision systems in terms of how they process visual information [7]. Computer vision applications for the automated detection of Parkinson's disease employ a range of handwriting image characteristics, including spiral and wave patterns. The combination of the Histogram of Oriented Gradients (HOG) method with KNN has proven capable of accurately classifying the handwriting of Parkinson's patients, with a classification accuracy of 89.33% [8]. The random forest method has demonstrated the capacity to accurately identify instances of Parkinson's disease in both spiral and wave images, exhibiting a sensitivity and specificity rate of 86.67 and 83.30%, respectively. These findings are supported by the existing literature [1]. The logistic regression method is also effective at classifying spiral images, with an accuracy rate of 91.6% [5]. The VGG-16 method has been shown to be effective in the detection of Parkinson's disease from micrographic static hand drawings, achieving a training accuracy of 90.63% and a testing accuracy of 91.36% [9]. One of the most frequently utilized artificial intelligence techniques for image classification is the convolutional neural network (CNN) method.

The principal benefit of this approach is that it enables the automatic extraction and classification of features without necessitating manual feature selection and extraction [10]. CNN architectures such as AlexNet, GoogleNet, VGG-16, LeNet5, ResNet-50 [11] and DenseNet-169 to recognize patterns from an image. A Continuous Convolution Network (CCN) has demonstrated an 89.3% accuracy in classifying spiral images [12]. In a comparative study of VGG16, VGG19, ResNet18, ResNet50, and ResNet101 methods for the early diagnosis of Parkinson's disease, Huang et al. observed that the latter four exhibited superior accuracy in classifying wave images relative to spiral images. The accuracy obtained was 92% for VGG16, 96.67% for VGG19, 92.67% for ResNet18, 87.33% for ResNet50, and 94% for ResNet101 [13]. Additionally, DenseNet-169 is distinguished by its robust architecture and is typified by dense connectivity, facilitating reuse of features and gradient flow [14]. DenseNet-169 can be classified based on its capacity to resolve the issue of vanishing gradients, its effective feature propagation strategy, its reduction of the number of trainable parameters, and its promotion of feature reuse [15]. The model's comparative popularity is enhanced by its larger size and improved accuracy [16]. DenseNet-169 is capable of classifying Pap smear images with an accuracy rate of 91.72% [14], images of peanut plant leaves with 99.83% [17], identifying lung disease using X-ray images with an accuracy rate of 91% [18] and is effective in detecting Alzheimer's disease through brain MRI images with an accuracy rate of 87% [16].

This research is based on existing literature, with the objective of applying the DenseNet-169 architecture to classify spiral and wave handwriting images for the early detection of Parkinson's disease. Additionally, it aims to compare the efficacy of this approach with that of other convolutional neural network (CNN) architectures.

2. Materials and Methods

The objective of this research is to develop a method for classifying spiral and wave image handwriting data for the purpose of early detection of Parkinson's disease (PD) using a DenseNet-169 architecture. The research comprises several stages, including:

1) Collection of handwriting image datasets from Parkinson's patients and normal patients,
2) Augmentation process,
3) Preprocessing,
4) Dataset separation,
5) Feature Learning, and
6) Results analysis method, as illustrated in Fig. 1.

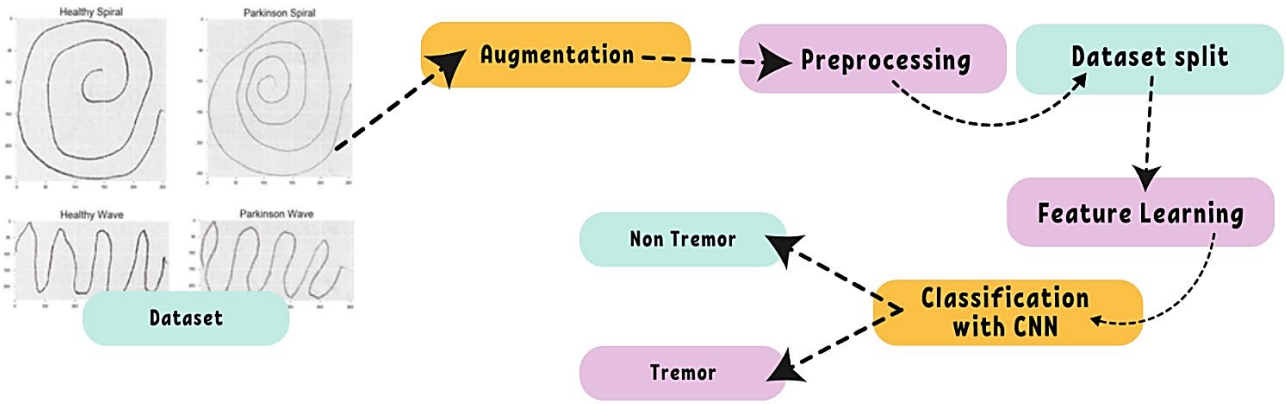

Fig. 1 *Phases of research*

Int. Journal of Integrated Engineering Vol. 17 No. 5 (2025) p. 363-375

2.1 Dataset Collection

The most crucial phase of the research process is the data collection stage, wherein the data utilized is of a secondary source, procured from the online repository https://www.kaggle.com/datasets/kmader/parkinsons-drawings. The data set comprises 27 patients with PD and 28 healthy controls from the Dandenong Neurology Clinic in Melbourne, Australia. The study was approved by the RMIT University Human Research Ethics Committee and conducted in accordance with the Declaration of Helsinki [19]. The data are images with a size of 256 x 256 pixels, comprising 102 spiral image data and 102 wave image data with an image length (m) of 512 pixels and an image width (n) exceeding 200 pixels. These images have been classified into two categories: tremor for PD patients and non-tremor for healthy patients (Fig. 2).

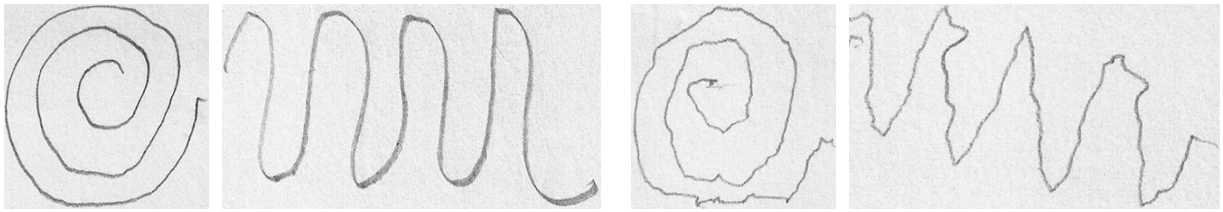

Non tremor Tremor

Fig. 2 *Spiral and wave pattern samples*

2.2 Augmentation

The augmentation stage is designed to enhance the diversity (variation) of data within the dataset [20] and to prevent overfitting during the training process of the DenseNet-169 model. The augmentation process involves the application of rotational transformations at three specific angles, namely 90°, 180°, and 270°, in addition to vertical flipping techniques (see Fig. 3). The augmentation process resulted in a significant increase in the amount of data, from 204 to 1020.

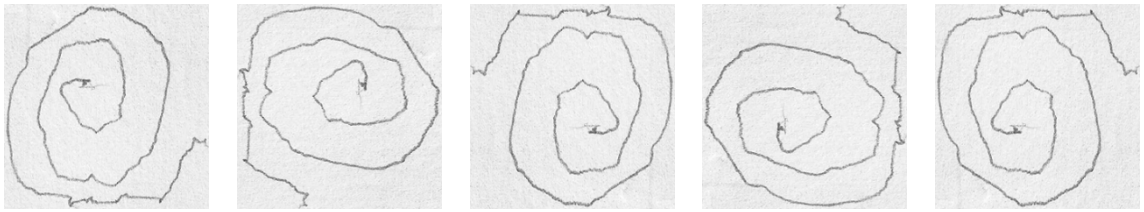

(a) **(b)** **(c)** **(d)** **(e)**

Fig. 3 *(a) Original spiral tremor image; (b) 90° rotation image; (c) 180° rotation image; (d) 270° rotation image; and (e) Vertical flipping image*

2.3 Preprocessing

The preprocessing stage is a stage used to enhance the quality of an image. Various techniques may be employed, including conversion to grayscale color space, application of a Gaussian blur, morphological erosion operations, addition of contrast, segmentation, and resizing of images. The procedure of converting to the greyscale color space is initiated by the separation of the channels within the RGB color space, followed by the application of the equation formula (1):

$$Grayscale\ (x,y) = 0.33\ R(x,y) + 0.33\ G(x,y) + 0.33\ B(x,y) \tag{1}$$

The variable x represents the area from the starting point inside the horizontal axis, the variable y represents the area from the starting point inside the vertical axis. The R variable represents the red channel value, the G variable represents the green channel value, and the B variable represents the blue channel value in the original image pixels. Moreover, the technique of Gaussian blurring was introduced as a means of simulating the effects of minor focal variations that can occur in actual diagnostic settings. Blurring has the potential to affect the clarity of structural boundaries within the image, as evidenced by research [21]. Gaussian filtering is performed according to the following equation (2):

$$G(x,y) = \frac{1}{2\pi\sigma^2} e^{-\frac{x^2+y^2}{2\sigma^2}} \tag{2}$$

The variable $\boldsymbol{x}$ represents the area from the starting point inside the horizontal axis, the variable $\boldsymbol{y}$ represents the area from the starting point inside the vertical axis, and the variable σ represents the standard deviation of

the Gaussian distribution [22]. Moreover, morphological operation techniques, such as erosion, are applied with the objective of removing extraneous noise while enhancing the clarity of the lines on objects that can be conceptualized as segments or regions within the image. The process entails the use of a structuring element (strel), which is analogous to an arbitrary-sized mask in image processing. The objective of the erosion operation is to reduce the size of the object segment by filling the perimeter of the object. The result will be smaller in proportion to the size of the strel used [23].

Binary images are typically subjected to erosion operations, although this technique may also be applied effectively to grayscale images, thereby enhancing the definition of the lines in the resulting image of grayscale handwriting. Subsequently, it is essential to introduce contrast in order to differentiate between the line (object) and the background by establishing a distinct gray level, as demonstrated by the equation formula (3)[24] :

$$contrast(x,y) = \frac{f(x,y) - min}{max - min} x1 \tag{3}$$

The next process is to separate the object from the background using segmentation techniques. The segmentation used is the Otsu thresholding technique, which is a technique that divides the histogram of a grayscale image into two different areas by determining the threshold variable (k) automatically by calculating the formula equation (4-9) [25], [26], [27], then the inverse process is performed using equation (10) to obtain a binary image, then the resize process is performed to normalize the data using the formula equation (11-12):

Find the probability of each pixel in the gray level of the image (i)

$$p_i = \frac{n_i}{N} \tag{4}$$

Calculating cumulative (ZerothCM)

$$\omega(k) = \sum_{i=0}^{k} p_i \tag{5}$$

Calculating cumulative mean (FirstCM)

$$\mu(k) = \sum_{i=0}^{k} i.p_i \tag{6}$$

Calculating global mean intensity (tMean)

$$\mu T = \sum_{i=0}^{L} i.p_i \tag{7}$$

The threshold value, k, is derived from the maximum value of the equation:

$$\sigma B^2(k^*) = \max\left(\sigma B^2(k)\right) \tag{8}$$

$$\sigma B^2(k^*) = \frac{[\mu \mathrm{T}.\mathrm{w}(\mathrm{k}) - (\mu(k)]^2}{w(k)[1 - w(k)]} \tag{9}$$

The inverse operation uses the equation:

$$biner\_invers(x,y) = 1 - f(x,y) \tag{10}$$

Resize image using equation:

$$m = \frac{pb * pp}{pa} \tag{11}$$

$$n = \frac{lb * pp}{la} \tag{12}$$

The variable m represents the new column pixel position, while n denotes the new row pixel position. The term pb signifies the new matrix length size, lb denotes the new matrix width size, and pp represents the old column pixel position. Additionally, pa denotes the length size of the old matrix, and la represents the width size of the old matrix.

Int. Journal of Integrated Engineering Vol. 17 No. 5 (2025) p. 363-375

2.4 Dataset Split

The data set is currently partitioned into three subsets: training data, testing data, and validation data. Researchers must carefully evaluate the size of datasets, train/test split ratios, and classification performance when splitting them into categories [28]. The optimal data ratio, as indicated by prior research (27, 9), is 80% training data, 10% testing data, and 10% validation data [29], [9]. The training set has 816 images, the validation and testing sets have 102 each, and the total data set is 1020. Additionally, the model was selected based on several factors, including the quantity of data utilized for training purposes. This approach is expected to enhance the model's capacity to recognize patterns within each class, thereby achieving a relatively high level of accuracy during the system testing phase.

2.5 DenseNet-169

Densenet169 is a principal image classifier developed by the Densenet group. Its popularity is enhanced by its larger size and enhanced accuracy [16]. The DenseNet169 architectural design comprises multiple layers, including convolutional, maxpool, dense, and transition layers [30] , as illustrated in Figure 4. The architectural design uses two activation functions: Relu and SoftMax. Relu is employed throughout architectural design, except for the final layer, where SoftMax is utilised instead. The purpose of the convolutional layer is to apply multiple filters to the image and generate a feature map which describes the intensity of the extracted features. To illustrate, if an image of dimensions L × N is subjected to a convolutional layer and an m × m filter is employed, the resulting convolution output will be of dimensions (1-m+1) x (1-n+1). Subsequently, the maxpool layer in DenseNet169 is employed to reduce the dimensionality of the feature map. Implementation of a pooling filter over the feature map results in the aggregation of features within the area covered by the filter region.

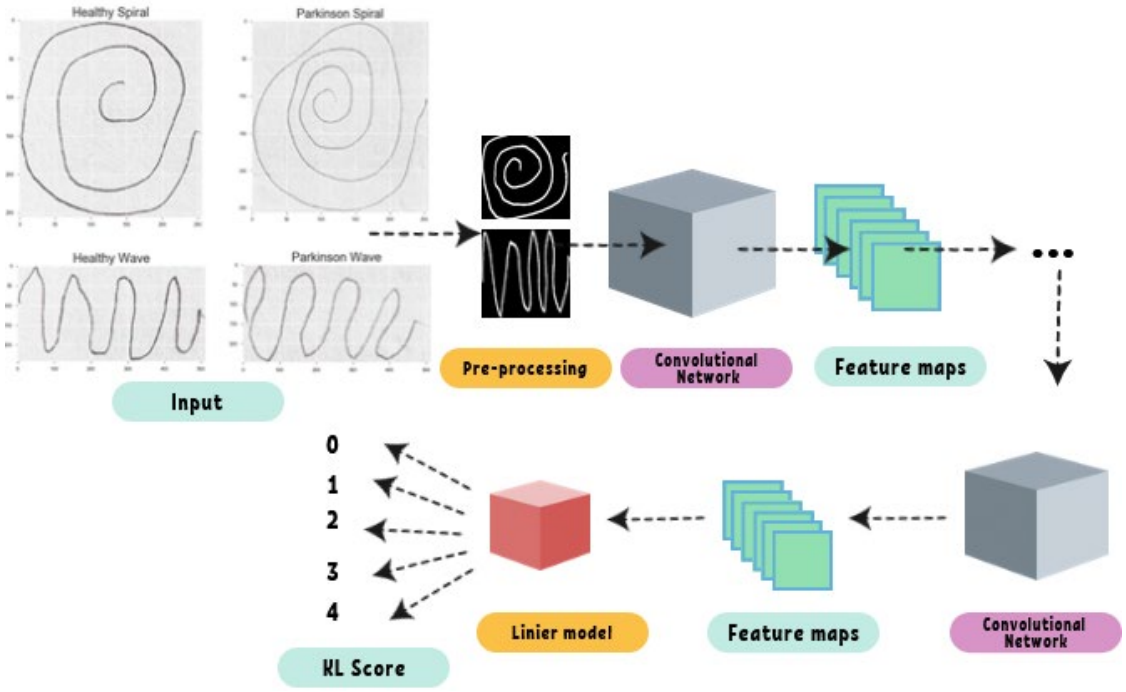

Fig. 4 *DenseNet-169 illustration*

MaxPool technique is calculated using the equation formula (11) where the feature map with (n_h, n_w, n_c) :

$$MaxPool = \frac{n_c x (n_h - f + 1) x (n_w - f + 1)}{S^2} \tag{11}$$

The variable c is used to indicate the channel of the feature map. Similarly, h indicates the height, w indicates the width, and f indicates the size of the filter. The DenseNet-169-layer architecture is described in Table 1.

Table 1 *DenseNet-169 architecture model*

Layer Name	Output Size	Densenet-169
Convolution	112 x 112	7 x 7 conv, stride 2
Pooling	56 x 56	3 x 3 max pool, stride 2
Dense Block 1	56 x 56	$\begin{bmatrix}1 \times 1 \text{ conv}\\3 \times 3 \text{ conv}\end{bmatrix} \times 6$
Transition Layer 1	56 x 56	1 x 1 conv
	28 x 28	2 x 2 average pool, stride 2
Dense Block 2	28 x 28	$\begin{bmatrix}1 \times 1 \text{ conv}\\3 \times 3 \text{ conv}\end{bmatrix} \times 12$
Transition Layer 2	28 x 28	1 x 1 conv
	14 x 14	2 x 2 average pool, stride 2
Dense Block 3	14 x 14	$\begin{bmatrix}1 \times 1 \text{ conv}\\3 \times 3 \text{ conv}\end{bmatrix} \times 32$
Transition Layer 3	14 x 14	1 x 1 conv
	7 x 7	2 x 2 average pool, stride 2
Dense Block 4	7 x 7	$\begin{bmatrix}1 \times 1 \text{ conv}\\3 \times 3 \text{ conv}\end{bmatrix} \times 32$
Classification Layer	1 x 1	7 x 7 global average pool
		1000D fully connected, softmax

3. Result

The preprocessing stage represents the most crucial phase in the handwriting image classification process. The objective of this process is to enhance the image quality to facilitate the CNN method with the DenseNet-169 architecture model in recognizing both spiral and wave handwriting patterns, which are essential for classifying tremor and non-tremor classes. The preprocessing stages include conversion to grayscale color space, Gaussian blur, image segmentation, and resizing. Color conversion from RGB to grayscale space is performed to facilitate segmentation, as the latter process can be challenging in an RGB color space with high value [31], [32]. The present research employs both spiral and wave images, which are initially converted to grayscale color space. Thereafter, they are subjected to a Gaussian filtering process, as detailed in the equation formula (2) illustrated in Fig. 5.

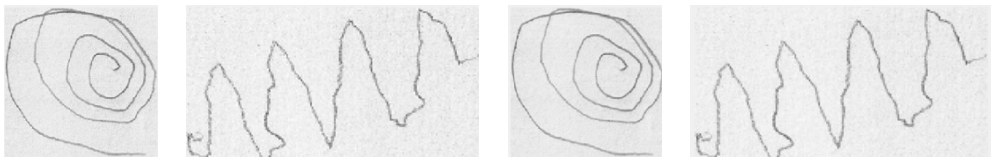

(a) **(b)** **(c)** **(d)**

Fig. 5 *(a - b) Grayscale image and (c - d) Gaussian filtering result image*

Gaussian filtering is employed for the purpose of image smoothing, which serves to enhance clarity and eliminate noise. To enhance the definition of the line, contrast is introduced through the implementation of the equation (3) and a morphological erosion operation (see Fig. 6).

(a) **(b)**

Fig. 6 *(a) Contrast image; and (b) Erosion morphology operation image*

Int. Journal of Integrated Engineering Vol. 17 No. 5 (2025) p. 363-375

Figure 6 illustrates the impact of contrast enhancement, which serves to clarify the lines in both the spiral and wave images. The morphological operation of erosion is designed to remove object points from the background. The effect observed in this image is the reduction of pixels with gray degree values, which results in the enlargement of pixels with a gray degree of 0. This process produces a discernible enhancement in the clarity of the lines visible in both spiral and wave images. The following process is the segmentation process, which employs the Otsu method with a T threshold value of 0.42. However, the binary image formed by the spiral and wave lines is 0, indicating black, while the background is 1, indicating white. Therefore, it is necessary to add another process, namely the inverse image technique (Fig. 7).

(a) **(b)**

Fig. 7 *Binary image (a) Otsu segmentation result; and (b) Inverse technique result*

This inverse technique aims to transform pixels that were originally assigned the numerical value of one (1) into zeroes (0), and vice versa. This process allows for the creation of objects in the form of lines that are white and assigned the numerical value of one (1). The binary image is subsequently resized to normalize the size of the spiral image and wave image, which are both 224 x 224 pixels in size (Fig. 8).

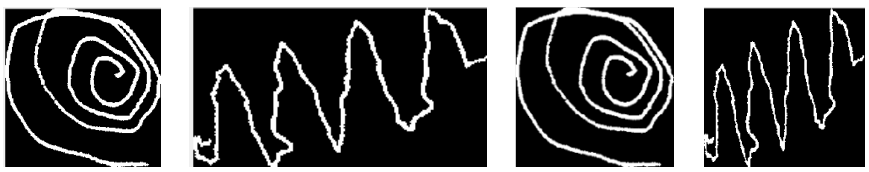

(a) **(b)**

Fig. 8 *Binary image (a) Before normalization; and (b) After normalization 224 x 224 pixels*

Following the acquisition of the normalized input image, it is necessary to proceed with the training of the dataset on the Google Collaboratory platform with the objective of achieving the distinction between two classes: namely, tremor and non-tremor. The training process for the dataset employs the DenseNet-169 architectural model, comprising 169 layers as indicated in Table 1. Two learning rate experiments were conducted as part of the training process, with learning rates of $\alpha = 0.001$ and $\alpha = 0.0001$. A range of maximum epochs was considered, from 10 to 60, for the purpose of obtaining system accuracy and loss validation, as detailed in Table 2.

Table 2 *A comparative analysis of the efficacy of the DenseNet-169 model with varying learning rates*

Epoch	$\alpha = 0.001$				$\alpha = 0.0001$			
	Accuracy	Val Accuracy	Loss	Val Loss	Accuracy	Val Accuracy	Loss	Val Loss
10	0.9596	0.8431	0.1208	1.8574	1.0000	0.9216	0.0035	0.3676
13	0.9853	0.7843	0.0509	1.5452	1.0000	0.9412	0.0016	0.3204
20	0.9804	0.8431	0.0563	0.8597	0.9975	0.9412	0.0048	0.2898
23	0.9816	0.8824	0.0654	2.4295	0.9988	0.9412	0.0027	0.2928
26	0.9951	0.9412	0.0209	0.3914	0.9939	0.9314	0.0200	0.3100
30	0.9963	0.9020	0.0237	0.6356	0.9828	0.9412	0.0521	0.4352
39	0.9926	0.9216	0.0167	0.7424	0.9951	0.8431	0.0163	1.1114
40	0.9975	0.9216	0.0084	0.6981	0.9914	0.9216	0.0438	0.3317
50	0.9841	0.7059	0.0605	2.7703	1.0000	0.9314	0.0010	0.5335
52	0.9755	0.8627	0.0688	0.7635	1.0000	0.9314	0.0006	0.5968
60	0.9951	0.9314	0.0071	0.9609	1.0000	0.9216	0.0003	0.6877

Training accuracy is an indicator of the model's performance on the training dataset. The use of the learning rate α = 0.001 with epoch = 10 results in a training accuracy of 95.96%. As the number of epochs increases, the accuracy of the system also increases until reaching a maximum at epoch 40, where it is 99.75%. In contrast to the use of a learning rate α = 0.0001, the system demonstrates 100% accuracy in training with an epoch value of 10. However, there is a notable decrease in the accuracy level when epoch values range from 20 to 40. It can be observed that when the epoch value ranges from 50 to 60, the system training accuracy exhibits a notable increase, reaching 100%. The training loss is a metric used to evaluate the performance of a deep learning model in fitting the training data. In other words, it evaluates the error rate of the model on the training set. The training loss exhibits fluctuations as the epoch increases when the learning rate is set to α = 0.001 and α = 0.0001. The lowest training loss observed at α = 0.001 is 0.0071 at epoch = 60, while at α = 0.0001, the lowest training loss is 0.0003.

Validation accuracy is a metric employed to assess the quality of a neural network classifier, specifically regarding its capability to accurately classify data sets that were not part of the training process. The validation accuracy values for the DenseNet-169 model with a learning rate α = 0.001 demonstrate a variable trend, with the highest recorded value of 94.12% occurring at epoch = 26. However, at the same epoch, DenseNet-169 with a learning rate α = 0.0001 achieved validation accuracy of 93.14%. The validation loss is analogous to the training loss and is calculated as the sum of errors for each example in the validation set. The results presented in Table 2 reveal that the validation loss at the learning rate α = 0.0001 is less than that observed at α = 0.001. Consequently, the learning rate identified as optimal for the system testing process is DenseNet169 with a learning rate α = 0.0001. To calculate accuracy, precision, recall and F1-score (Table 3), the system is obtained based on the calculations in the confusion matrix table, as illustrated in Figure 9.

PREDICTED

ACTUAL	Non Tremor	Tremor
Non Tremor	49	1
Tremor	6	46

Fig. 9 *Result of confusion matrix*

Table 3 *Results of system performance with a learning rate α = 0.0001 and image preprocessing*

Class	Precision	Recall	F1-Score
Non Tremor	0.89	0.98	0.93
Tremor	0.98	0.88	0.93
Accuracy			0.93

Precision is an indicator of the percentage of predictions as positive classes that are positive. Recall or sensitivity is an indicator of the percentage of total classes predicted to be positive, known as the true positive rate (TPR) [33]. The precision of the system in recognising the non-tremor class image is less than the tremor class, with a value of 0.89, while the recall result for the tremor class is 0.88. The F1 score is a value indicator that considers both false positives and false negatives, giving a value of 0.93 or 93%, which indicates the accuracy of the system. In this study, the training accuracy exceeds the testing accuracy, which is evidence of overfitting, as demonstrated in the graph (Fig.10).

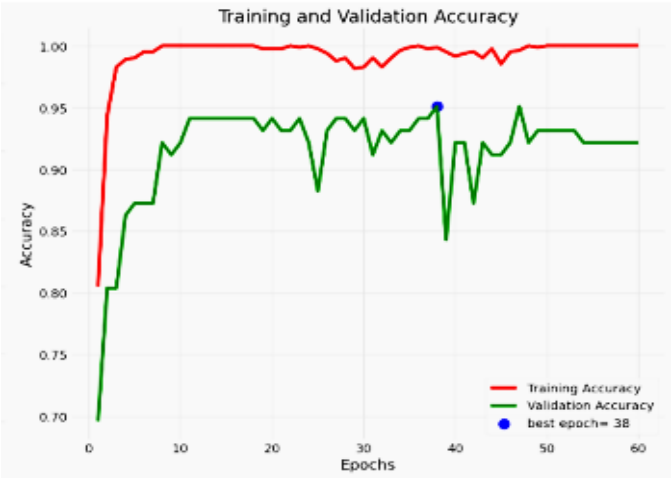

Fig. 10 *Training and testing accuracy graph*

Int. Journal of Integrated Engineering Vol. 17 No. 5 (2025) p. 363-375

Despite the overfitting of our model results, we have validated the importance of image preprocessing. Furthermore, we conducted training and testing with images that lacked preprocessing, as illustrated in the confusion matrix (Fig. 11) and system performance results (Table 4).

PREDICTED

ACTUAL	Non Tremor	Tremor
Non Tremor	43	7
Tremor	12	40

Fig. 11 *Result of confusion matrix*

Table 4 *Results of system performance with a learning rate α = 0.0001 without image preprocessing*

Class	Precision	Recall	F1-Score
Non Tremor	0.78	0.86	0.82
Tremor	0.85	0.77	0.81
Accuracy			0.81

Table 4 illustrates that the precision of the system in identifying the non-tremor class is less accurate than in recognising the tremor class, with a value of 0.78, whereas the recall result for the tremor class is 0.77. The F1-score for the non-tremor class is 0.82, and the tremor class is 0.81, resulting in an overall system accuracy of 81%. Furthermore, the efficacy of the DenseNet-169 method was evaluated on spiral images under two distinct conditions: (a) augmentation and (b) additional preprocessing as outlined in Table 5. The performance outcomes of DenseNet-169 on wave images are detailed in Table 6. The two processes were tested with a maximum of 30 epochs.

Table 5 *System performance results on spiral images*

Class	Precision		Recall		F1-Score	
	(a)	(b)	(a)	(b)	(a)	(b)
Non Tremor	0.95	0.94	0.76	0.68	0.84	0.79
Tremor	0.81	0.76	0.96	0.96	0.88	0.85
Accuracy					0.86	0.82

Table 5 illustrates that DenseNet-169 encounters challenges in both classification and accurate identification of spiral images belonging to the Tremor class when utilizing (a) augmentation and (b) preprocessing techniques. It is evident that augmentation has a significant impact on system accuracy, with a rate of 86%. Conversely, the combination of augmentation and preprocessing has an accurate rate of 82%. The present test differs from the results of the system's performance when classifying and identifying wave images. As illustrated in Table 6, an evident enhancement in system accuracy is observed when wave images are augmented through preprocessing, reaching an accuracy rate of 84%. Conversely, when solely relying on the augmentation process, the system accuracy is 65%. The preprocessing stage is the most crucial in both tests, as it helps to differentiate between images that are similar in appearance. It is therefore necessary to select spiral image data and wave images for the purpose of early detection of Parkinson's disease.

Table 6 *System performance results on wave images*

Class	Precision		Recall		F1-Score	
	(a)	(b)	(a)	(b)	(a)	(b)
Non Tremor	1.00	0.78	0.31	0.96	0.47	0.86
Tremor	0.58	0.96	1.00	0.72	0.74	0.82
Accuracy					0.65	0.84

4. Discussion

The results are also compared with several reference journals, as detailed in Table 5 for reference. The references utilized in our study, besides comparing methodologies, also include a literacy review related to the development of research on early detection of Parkinson's with spiral and wave images. Some references have been found to

utilize disparate datasets from the one employed in our study; however, it is necessary to understand the detection of early Parkinson's disease through the analysis of spiral and wave patterns in handwriting.Intelligent methods, such as convolutional neural networks (CNNs), employ pattern recognition to classify spiral or wave patterns in handwriting. This classification is unaffected by variations in datasets, provided that the spiral and wave writing patterns remain consistent.

The research of Y. Huang et al. serves as the primary reference point for our study. This research implements preprocessing techniques, including AugMix, which involves geometric transformation and pixel manipulation for the purpose of image augmentation [34]. This method eliminates image enhancement processes, including contrast, color conversion, brightness, sharpness, and cutout operations.Subsequently, images that have undergone AugMixed processing are subjected to classification through the utilization of multiple CNN architectures. In this study, the CNN model with VGG16 architecture is the most effective at classifying the wave image dataset, achieving an accuracy of 90%. In contrast, the spiral image is most accurately classified by Resnet18, with an accuracy of 86.67% [13]. Therefore, we employ image enhancement techniques such as Gaussian blur, as well as morphological operations of erosion and contrast enhancement. The results of our research, as compared to the relevant literature, are presented in Table 7.

Table 7 *A comparison of research results*

Author	Research Methods	Result and Evaluation
Ferdib-Al-Islam and L. Akter [8]	Combination of the Histogram of Oriented Gradients (HOG) method with KNN	The system was able to classify the handwriting of Parkinson's patients with an accuracy of 89.33%.
N. M. Ranjan et al[1]	Combination of Histogram of Oriented Gradients (HOG) method with Random Forest Classifier	The system can classify the handwriting of Parkinson's patients with an accuracy of 86.67% for spiral images and 83.30% for wave images.
M. Kamble et al[5]	Logistic Regression	The system can classify spiral images into two classes healthy and stroke with an accuracy rate of 91.6%.
N. Basnin et al[9]	VGG-16	This method can detect Parkinson's disease from Micrographic Static Hand Drawings with a training accuracy of 90.63% and a testing accuracy of 91.36%.
Z. Li et al[12]	Continuous Convolution Network (CC-Net)	This method can classify spiral images with an accuracy of 89.3%.
Y. Huang et al[13]	Preprocessing : AugMix VGG16, VGG19, ResNet18, ResNet50 and ResNet101	In this study, the accuracy of the system in classifying spiral images and wave images: VGG16 : 90% (wave) and 83.33% (spiral); VGG19 : 86.67% (wave) and 80% (spiral); ResNet18 : 90% (wave) and 86.67% (spiral); ResNet50 : 76.67% (wave) and 83.33% (spiral); and ResNet101 : 84.67% (wave) and 81.33% (spiral).
Proposed	Preprocessing: conversion to grayscale colour space, Gaussian blur, morphological operations of erosion, contrast enhancement, segmentation and image resizing Machine Learning: DenseNet-169	DenseNet-169 can classify spiral and wave images in tremor and non-tremor classes with the addition of preprocessing obtained a training accuracy of 100%. the system test accuracy is 93% (Table 3) while without preprocessing, the system accuracy is 81% (Table 4).

As illustrated in Table 7, our research has demonstrated the significance of preprocessing in the augmentation process. The efficacy of our proposed technique is evident in its substantial impact on the accuracy rate of the DenseNet169 model in classifying spiral and wave images. The implementation of our proposed preprocessing technique results in an accuracy rate of 93%, while the system without this technique achieves an accuracy rate of 81%. However, the augmentation process is recommended for the classification of spiral images, as it achieves an accuracy rate of 86%. In contrast, the preprocessing technique is particularly beneficial for the classification of wave images, as it enhances the accuracy from 65% (without augmentation) to 84%.

5. Conclusion

This research aims to classify spiral and wave handwriting images for early detection of Parkinson's disease using DenseNet-169. A key finding of this study is that the image preprocessing stage is of critical importance, as it

enables the clarification of patterns in spiral and wave images, enhancing the efficacy of the CNN classification process with DenseNet-169. This is confirmed by a significant enhancement in accuracy, whereby classification without preprocessing results in a system accuracy rate of 81%, while the proposed preprocessing leads to an elevated system accuracy rate of 93%. A comparison of previous research with VGG-16 and DenseNet-169 reveals that the DenseNet-169 model exhibits superior accuracy, with a 93% accuracy percentage, as opposed to the 90.63% accuracy observed in the VGG-16 model. The results are influenced by misclassified data, which may be caused by the large amount of similar data between tremor classes and non-tremor classes, especially in spiral images. Therefore, additional data is an important factor for further system development. It is also necessary to compare several augmentation techniques as data preprocessing before being classified by the CNN model.

Acknowledgement

This research project has been funded by LP2M University of Jember (Grant Number 7554/UN25/KP/2024) as part of the KeRis-DiMas Grant Year 2024 scheme. My gratitude extends to dr. Ahdinar Rosdiana Dewi, Sp.N and Alfian Pramudita Putra ST, M.Sc, who provided invaluable assistance with user acceptance testing on our website application.

Conflict of Interest

Authors declare that there is no conflict of interest regarding the publication of the paper.

Author Contribution

The authors confirm contribution to the paper as follows: ***study conception and design:*** *Arizal Mujibtamala Nanda Imron, Wahyu Muldayani and Sumardi;* ***data collection and web development:*** *Azizatul Mashwafah;* ***analysis and interpretation of results:*** *Zilvanhisna Emka Fitri;* ***draft manuscript preparation*** *Arizal Mujibtamala Nanda Imron, Zilvanhisna Emka Fitri and Azizatul Mashwafah. All authors reviewed the results and approved the final version of the manuscript.*

References

[1] N. M. Ranjan, G. Mate, and M. Bembde, "Detection of Parkinson's Disease using Machine Learning Algorithms and Handwriting Analysis," *JoDMM*, vol. 8, no. 1, pp. 21–29, Mar. 2023, doi: 10.46610/JoDMM.2023.v08i01.004.

[2] M. Hamdan, A. P. Suharto, P. Nugraha, and W. R. Islamiyah, "Motor improvement in Parkinson's disease patients receiving caffeine adjuvants: A double-blind randomized controlled trial in Indonesia," *Narra J*, vol. 4, no. 2, p. e826, Jul. 2024, doi: 10.52225/narra.v4i2.826.

[3] L. S. Bernardo *et al.*, "Handwritten pattern recognition for early Parkinson's disease diagnosis," *Pattern Recognition Letters*, vol. 125, pp. 78–84, Jul. 2019, doi: 10.1016/j.patrec.2019.04.003.

[4] P. K. Handayani, "Penerapan Algoritma Support Vector Machine (SVM) Untuk Analisis Pola Klasifikasi Pada Parkinson's Dataset," *IJTIS*, vol. 3, no. 1, pp. 31–35, Dec. 2021, Accessed: Jan. 24, 2024. [Online]. Available: https://doi.org/10.24176/ijtis.v3i1.7530

[5] M. Kamble, P. Shrivastava, and M. Jain, "Digitized spiral drawing classification for Parkinson's disease diagnosis," *Measurement: Sensors*, vol. 16, p. 100047, Aug. 2021, doi: 10.1016/j.measen.2021.100047.

[6] S. Chakraborty, S. Aich, Jong-Seong-Sim, E. Han, J. Park, and H.-C. Kim, "Parkinson's Disease Detection from Spiral and Wave Drawings using Convolutional Neural Networks: A Multistage Classifier Approach," in *2020 22nd International Conference on Advanced Communication Technology (ICACT)*, Phoenix Park, PyeongChang,, Korea (South): IEEE, Feb. 2020, pp. 298–303. doi: 10.23919/ICACT48636.2020.9061497.

[7] A. D. Firmansyah, S. B. Kahar, and Z. E. Fitri, "Diabetic Retinopathy Severity Level Detection Using Convolution Neural Network," *eltikom*, vol. 8, no. 1, pp. 66–74, Jun. 2024, doi: 10.31961/eltikom.v8i1.1112.

[8] Ferdib-Al-Islam and L. Akter, "Early Identification of Parkinson's Disease from Hand-drawn Images using Histogram of Oriented Gradients and Machine Learning Techniques," in *2020 Emerging Technology in Computing, Communication and Electronics (ETCCE)*, Bangladesh: IEEE, Dec. 2020, pp. 1–6. doi: 10.1109/ETCCE51779.2020.9350870.

[9] N. Basnin, T. A. Sumi, M. S. Hossain, and K. Andersson, "Early Detection of Parkinson's Disease from Micrographic Static Hand Drawings," in *Brain Informatics*, vol. 12960, M. Mahmud, M. S. Kaiser, S. Vassanelli, Q. Dai, and N. Zhong, Eds., in Lecture Notes in Computer Science, vol. 12960. , Cham: Springer International Publishing, 2021, pp. 433–447. doi: 10.1007/978-3-030-86993-9_39.

[10] P. Y. Lo and S. L. Lim, "Atmospheric Cloud Image Detection with Convolutional Neural Network (CNN)," vol. 16, no. 3, 2024.

[11] G. S. Nugraha, M. I. Darmawan, and R. Dwiyansaputra, "Comparison of CNN's Architecture GoogleNet, AlexNet, VGG-16, Lenet -5, Resnet-50 in Arabic Handwriting Pattern Recognition," *KINETIK*, May 2023, doi: 10.22219/kinetik.v8i2.1667.

[12] Z. Li, J. Yang, Y. Wang, M. Cai, X. Liu, and K. Lu, "Early diagnosis of Parkinson's disease using Continuous Convolution Network: Handwriting recognition based on off-line hand drawing without template," *Journal of Biomedical Informatics*, vol. 130, p. 104085, Jun. 2022, doi: 10.1016/j.jbi.2022.104085.

[13] Y. Huang, K. Chaturvedi, A.-A. Nayan, M. H. Hesamian, A. Braytee, and M. Prasad, "Early Parkinson's Disease Diagnosis through Hand-Drawn Spiral and Wave Analysis Using Deep Learning Techniques," *Information*, vol. 15, no. 4, p. 220, Apr. 2024, doi: 10.3390/info15040220.

[14] D. B. Talpur, A. R. Rang, A. Khowaja, and A. Shah, "DeepCervixNet: An Advanced Deep Learning Approach for Cervical Cancer Classification in Pap Smear Images," *VAWKUM Transactions on Computer Sciences*, vol. 12, no. 1, pp. 136–148, 2024.

[15] Y. M. Malgwi, S. S. Wagbe, S. D. A. Abdulkadir, and L. C. Okpalaifeako, "An Improved Intrusion Detection System Using Densenet," *International Journal of Current Researches in Sciences, Social Sciences and Languages*, vol. 04, no. 02, pp. 4–18, 2024.

[16] K. Ashwini, K. Valarmathi, B. Vanipriya, and M. Devi, "Alzheimer's disease detection using deep neural network in densenet 169," in *Proceedings of the 6th International Conference on Intelligent Computing (ICIC-6 2023)*, vol. 107, A. K. Visvam Devadoss, M. Subramanian, V. Emilia Balas, F. A. Turjman, and R. Malaichamy, Eds., in Advances in Computer Science Research, vol. 107. , Dordrecht: Atlantis Press International BV, 2024, pp. 20–25. doi: 10.2991/978-94-6463-250-7_5.

[17] A. M. P. and A. P. Reddy, "Dataset of groundnut plant leaf images for classification and detection," *Data in Brief*, vol. 48, p. 109185, Jun. 2023, doi: 10.1016/j.dib.2023.109185.

[18] K. Nair, A. Deshpande, R. Guntuka, and A. Patil, "Analysing X-Ray Images to Detect Lung Diseases Using DenseNet-169 technique," *SSRN Journal*, 2022, doi: 10.2139/ssrn.4111864.

[19] P. Zham, D. K. Kumar, P. Dabnichki, S. Poosapadi Arjunan, and S. Raghav, "Distinguishing Different Stages of Parkinson's Disease Using Composite Index of Speed and Pen-Pressure of Sketching a Spiral," *Front. Neurol.*, vol. 8, p. 435, Sep. 2017, doi: 10.3389/fneur.2017.00435.

[20] L. Wei Yong, R. Ambar, M. H. Abd Wahab, M. M. Abd Jamil, and C. Chang Choon, "Detection and Measurement System for Button Mushrooms Using Convolutional Neural Network," *IJIE*, vol. 16, no. 1, pp. 262–271, Apr. 2024, doi: 10.30880/ijie.2024.16.01.021.

[21] Y. Kumaran S, J. J. Jeya, M. T. R, S. B. Khan, S. Alzahrani, and M. Alojail, "Explainable lung cancer classification with ensemble transfer learning of VGG16, Resnet50 and InceptionV3 using grad-cam," *BMC Med Imaging*, vol. 24, no. 1, p. 176, Jul. 2024, doi: 10.1186/s12880-024-01345-x.

[22] R. Shukla and L. Shrivastava, "Image Restoration of Image with Gaussian Filter," *International Research Journal of Engineering and Technology (IRJET)*, vol. 07, no. 12, pp. 555–558, 2020.

[23] I. P. E. Sutariawan, G. R. Dantes, and K. Y. Ernanda Aryanto, "SEGMENTASI MATA KATARAK PADA CITRA MEDIS MENGGUNAKAN METODE OPERASI MORFOLOGI," *JIK*, vol. 3, no. 1, pp. 23–31, Sep. 2019, doi: 10.23887/jik.v3i1.2750.

[24] Z. E. Fitri, F. A. Pramudya, and A. M. N. Imron, "Implementation of Channel Area Thresholding in Early Detection System of Acute Respiratory Infection (ARI)," *IAPL*, vol. 5, no. 1, pp. 14–22, May 2024, Accessed: Sep. 04, 2024. [Online]. Available: https://doi.org/10.20473/iapl.v5i1.55626

[25] Katherine, R. Rulaningtyas, and K. Ain, "CT scan image segmentation based on hounsfield unit values using Otsu thresholding method," *J. Phys.: Conf. Ser.*, vol. 1816, no. 1, p. 012080, Feb. 2021, doi: 10.1088/1742-6596/1816/1/012080.

[26] Q. Cao, L. Qingge, and P. Yang, "[Retracted] Performance Analysis of Otsu-Based Thresholding Algorithms: A Comparative Study," *Journal of Sensors*, vol. 2021, no. 1, p. 4896853, Jan. 2021, doi: 10.1155/2021/4896853.

[27] M. Edupuganti, V. Rathikarani, and K. Chaduvula, "A Real and Accurate Ultrasound Fetal Imaging Based Heart Disease Detection Using Deep Learning Technology," *IJIE*, vol. 14, no. 7, pp. 56–68, Dec. 2022, doi: 10.30880/ijie.2022.14.07.005.

[28] I. O. Muraina, "Ideal Dataset Splitting Ratios In Machine Learning Algorithms: General Concerns For Data Scientists And Data Analysts," in *7th International Mardin Artuklu Scientific Researches Conference*, Mardin: www.artuklukongresi.org, 2021. [Online]. Available: https://www.researchgate.net/profile/Ismail-Muraina/publication/358284895_IDEAL_DATASET_SPLITTING_RATIOS_IN_MACHINE_LEARNING_ALGORITHMS_GENERAL_CONCERNS_FOR_DATA_SCIENTISTS_AND_DATA_ANALYSTS/links/61fb97e711a1090a79cc1a8b/IDEAL-DATASET-SPLITTING-RATIOS-IN-MACHINE-LEARNING-ALGORITHMS-GENERAL-CONCERNS-FOR-DATA-SCIENTISTS-AND-DATA-ANALYSTS.pdf

[29] P. Khatamino, I. Canturk, and L. Ozyilmaz, "A Deep Learning-CNN Based System for Medical Diagnosis: An Application on Parkinson's Disease Handwriting Drawings," in *2018 6th International Conference on Control Engineering & Information Technology (CEIT)*, Istanbul, Turkey: IEEE, Oct. 2018, pp. 1–6. doi: 10.1109/CEIT.2018.8751879.

[30] B. A. S. Al-rimy, F. Saeed, M. Al-Sarem, A. M. Albarrak, and S. N. Qasem, "An Adaptive Early Stopping Technique for DenseNet169-Based Knee Osteoarthritis Detection Model," *Diagnostics*, vol. 13, no. 11, p. 1903, May 2023, doi: 10.3390/diagnostics13111903.

[31] R. H. Ariesdianto, Z. E. Fitri, A. Madjid, and A. M. N. Imron, "Identifikasi Penyakit Daun Jeruk Siam Menggunakan K-Nearest Neighbor," *Jur. Ilm. Komp. & Infor.*, vol. 1, no. 2, pp. 133–140, Nov. 2021, doi: 10.54082/jiki.14.

[32] B. A. Prasetya, Z. E. Fitri, A. Madjid, and A. M. N. Imron, "Ensiklopedia Digital Varietas Ubi Jalar Berdasarkan Klasifikasi Citra Daun Menggunakan KNearest Neighbor," *elektrika*, vol. 14, no. 1, p. 1, Apr. 2022, doi: 10.26623/elektrika.v14i1.4329.

[33] A. M. N. Imron, Z. E. Fitri, B. Hasan, and R. Y. Widiastuti, "Web-based Learning Media for Alphabet Recognition in Early Childhood using LeNet-5," *Journal of Information Systems Research and Practice*, vol. 2, no. 3, pp. 32–43, 2024.

[34] M. Xu, S. Yoon, A. Fuentes, and D. S. Park, "A Comprehensive Survey of Image Augmentation Techniques for Deep Learning," *Pattern Recognition*, vol. 137, p. 109347, May 2023, doi: 10.1016/j.patcog.2023.109347.